2023 IEEE International Conference on Robotics and Automation (ICRA 2023)
May 29 - June 2, 2023. London, UK

A New Sensation: Digital Strain Sensing for Disturbance Detection In Flapping Wing Micro Aerial Vehicles

Regan Kubicek[1], Mahnoush Babaei[2], Alison I. Weber[3], and Sarah Bergbreiter[1]

***Abstract*— Flapping wing micro aerial vehicles face challenges in sensing and reacting to disturbances like wind gusts. This work introduces a new microscale bio-inspired digital strain sensor to detect these perturbations. The sensor is designed to change logic states when a specified strain threshold has been reached. The sensors are 3D printed on a flexible Mylar wing using two-photon polymerization. Three digital sensors with varying strain thresholds demonstrate differences in activation timing due to different design parameters. The sensors are tested at the 25 Hz flapping frequency of a hawkmoth, an insect with comparable wing size. A perturbation was added to the flapping wing by subjecting it to a 3 m/s wind gust. A single digital sensor is able to identify the wind disturbance by comparing the time of the first strain threshold crossing. A separate approach looks at the change in sensor 'on'-time for each flap cycle and provides a clear indication of the wind disturbance.**

I. INTRODUCTION

Microscale flapping wing robots and flying insects suffer similar constraints in size, weight, and power (SWAP) [1]. However, biology presents thousands of species that have overcome these barriers and demonstrate mastery of flight in a dynamic environment. Insect-scale flapping wing micro aerial vehicles (FWMAVs) range in size from a large butterfly such as the DelFly Nimble [2] to an order of magnitude smaller, as small as a bee [3]. One of the major challenges these micro-robotic systems face in moving outside of the lab is their inability to sense disturbances like wind gusts with sufficient time to recover. Due to their small size and low inertia, flapping wing MAVs are extremely susceptible to these perturbations. But we can look for inspiration from flying insects to develop new sensing strategies to handle fast-acting perturbations.

In this study, we model wings and sensors based on the properties of the hawkmoth (*Manduca sexta*). The hawkmoth takes advantage of multiple sensing modalities, such as vision and mechanosensory feedback, for use in flight control. For instance, the moth's antennae are able to sense Coriolis forces [4] and detect wind gusts [5]. The moth's vision is used for flight stability and is useful in slower flight maneuvers [6]. To respond to fast perturbations such as wind gusts, the hawkmoth, and other flying insects are richly equipped with biological strain sensors called campaniform sensilla (CS) on the top and bottom of their wings [7]. During wing deformations, the CS deform and activate neurons that generate action potentials in response to strain [8]. These neurons are extremely fast, and fire with sub-millisecond precision [9]. In this work, we draw inspiration from these mechanosensors to develop bio-inspired digital strain sensors capable of detecting wind gusts within a single flap cycle.

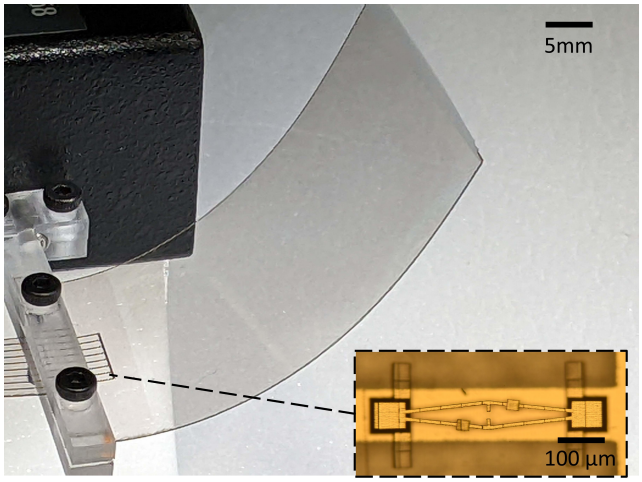

Fig. 1. Fabricated wing with 7 strain sensors. The inset shows a microsope image of the 3D printed digital strain sensor.

The use of sensors on the wings of aerial vehicles to detect disturbances and aerodynamic forces has been demonstrated on larger fixed wing [10], and rotary aircraft [11]. However, there are significant challenges when designing sensing systems for insect-scale FWMAVs. To achieve full autonomy, sensors must be integrated with the FWMAV's control system [12]. An ideal sensor would be low latency and easily integrated with a microcontroller unit (MCU) without additional hardware. In previous work, a discrete analog strain sensor was developed but was still relatively large and stiff for small flapping wing MAVs. This paper builds on this idea to provide a completely digital strain threshold sensor that is $\approx 500\,\mu m$ in length and can easily be integrated onto flexible wings.

The primary contribution of this paper is a digital, bio-inspired strain sensing design. These novel temporal sensors can be used to infer the magnitude of disturbances without directly encoding strain itself but instead by encoding the

This research effort was supported by NSF GRFP DGE1745016/ DGE2140739, the Air Force Office of Scientific (AFOSR) Research MURI award number FA9550-19-1-0386, and the Washington Research Foundation. The authors would also like to recognize prior support from the AFOSR grant FA9550-14-1-0398 to S. Bergbreiter and T. Daniel.

[1]Department of Mechanical Engineering, Carnegie Mellon University, Pittsburgh, PA, USA.
[2]Department of Aerospace Engineering and Engineering Mechanics, The University of Texas at Austin, Austin, TX, USA.
[3]Department of Biology, University of Washington, Seattle, WA, USA.
*rkubicek@andrew.cmu.edu

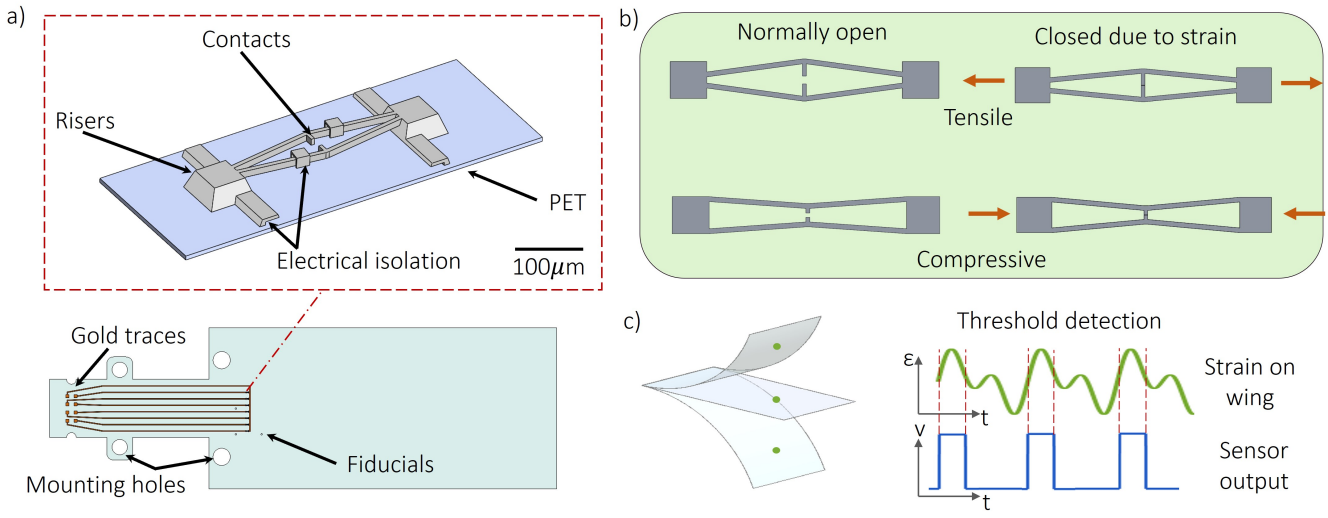

Fig. 2. Digital strain sensor concept. a) The chevron beams are lifted off the substrate with risers. Overhangs are directly incorporated into the design and provide electrical isolation. The sensors are directly 3D printed on a PET wing. Gold is deposited to provide electrical conductivity. b) The sensor is normally open and acts as a switch, closing at a specific strain threshold. The beams of the sensor can be configured to detect tensile and compressive strains. c) During the flapping cycle of the wing, the sensor is activated at a designed strain threshold. This provides mechanical filtering of the wing's strain and generates a digital signal.

timing at which a particular strain value is reached. An analytical model of the sensor's strain threshold is presented as a general guide for sensor design. A secondary contribution of this work is the fabrication of microscale sensors on flexible moth-sized wings (Fig.1). Rapid prototyping of the wing and sensor is accomplished through a novel fabrication technique that employs the use of microscale 3D printing. When the wings with printed sensors are flapped and subjected to wind gusts, the signal generated by the sensors can easily distinguish the onset of a wind gust within a wingbeat by analyzing changes in the digital signal.

II. METHODS

A. Sensor Design

The sensor was designed to detect and output a binary response to a strain threshold being crossed in a flapping wing . This required developing a sensor that could be incorporated into the wing and withstand strains throughout the flapping cycle when the wing is flapped at 25 Hz. In addition, the sensor should be sensitive enough to detect the relatively small strains experienced in thin, flexible wings and should not affect the stiffness and overall performance of the wing.

The sensor design (Fig. 2) is comprised of two chevron-shaped fixed-end beams that provide a mechanical gain with respect to displacement [13]. This mechanical amplification is needed to turn small strains in the wing into a detectable displacement. The chevron beams are lifted off of the substrate with risers to allow motion unconstrained by the substrate (Fig. 2a). The risers will also provide an additional mechanical gain on bent surfaces by extending the distance from the neutral axis of the bent wing. When the substrate undergoes a longitudinal strain, the beams amplify this displacement causing the contacts centered on each chevron to touch once a given displacement has been reached. The beams can be configured to detect a strain threshold due to either tensile or compressive strain in the substrate (Fig. 2b). All results in this paper utilize the tensile strain configuration.

The flapping motion of the wing causes large strains in the substrate that are cyclical based on the flapping frequency. The sensors are designed to open and close around a specific strain threshold. The sensor is coupled with a pull-down resistor to output a square wave (rising edge when closed, falling edge when open). The main benefit of using a contact-based sensor over traditional analog sensors is the signal-to-noise ratio. Traditional strain sensing approaches capture an analog signal using a Wheatstone bridge circuit and amplify it along with noise in the system. The noise must be filtered to obtain a usable signal. This amplification and signal processing takes up space, time, computational power, and electric power. The digital strain sensor, on the other hand, has a binary output, and the signal can be measured directly using the digital pin on a microcontroller where the sampling rate is not limited by an analog-to-digital converter (ADC) but instead by the clocking speed of the MCU's processer. This unique approach to measuring dynamic strain in a substrate creates a type of mechanical filtering in response to the flapping strain as shown in Fig. 2c.

B. Analytical Model

A kinematic model of the sensor provides a target strain as a function of the sensor's geometrical design parameters. A schematic of the kinematic relationship between the design parameters is shown in Fig. 3. Assuming no shrinkage/extension in chevron-shaped beams during fabrication, the length of a half of the beam, L, can be expressed in

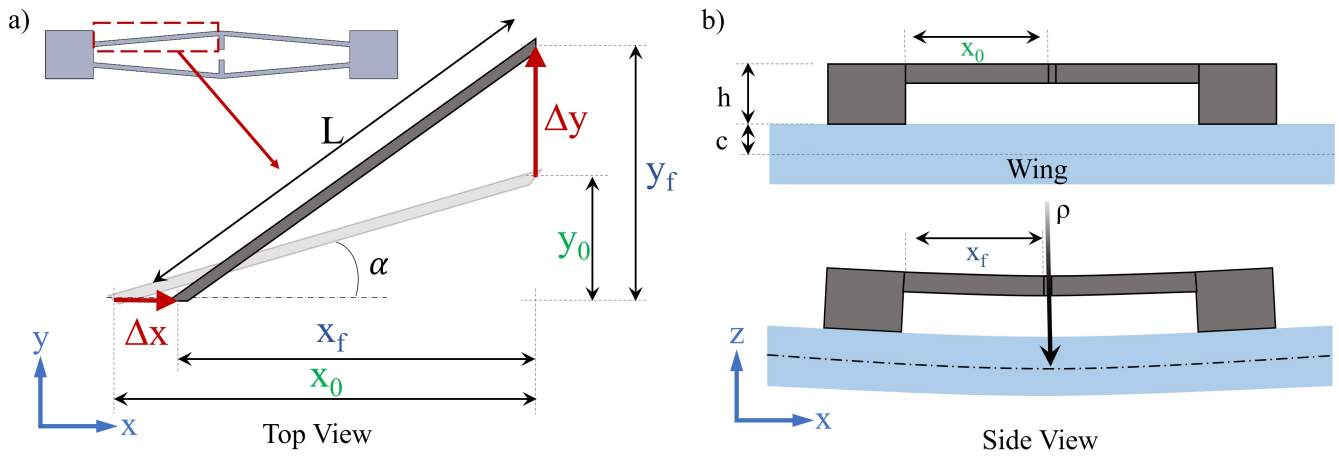

Fig. 3. Sensor schematic. a) The kinematic movement of the sensor beam relates displacement in the longitudinal (x) axis to the transverse (y) axis. b) A side view (along y+ axis) of the sensor demonstrates bending strain in the substrate that affects the longitudinal displacement of the sensor.

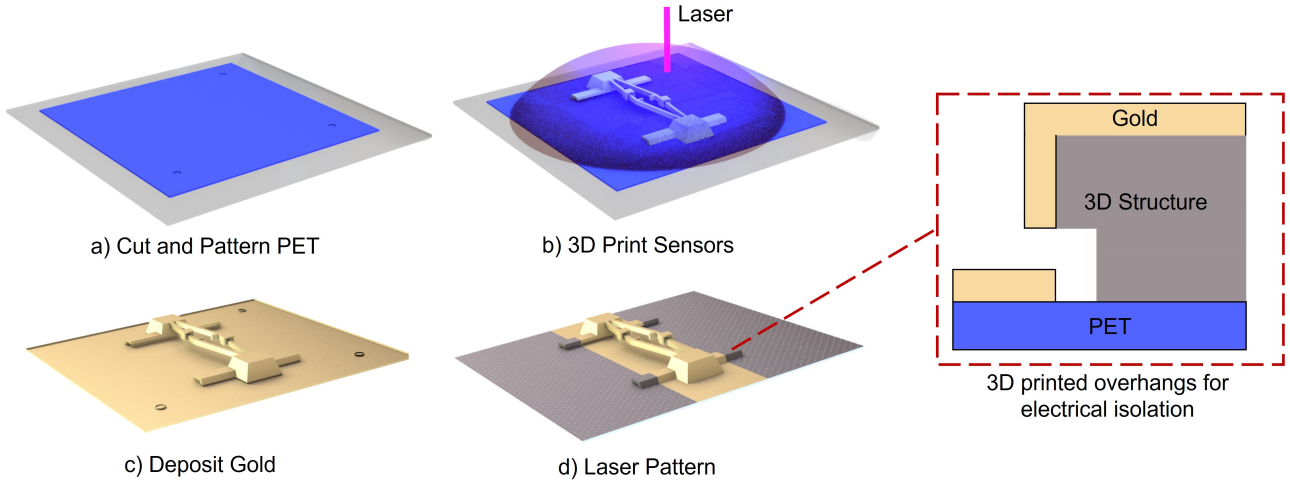

Fig. 4. Sensor fabrication. a) The PET wing is laser cut and adhered to a glass wafer. b) The sensors are printed in IP-S photoresist directly on the PET using two-photon polymerization. c) Gold is sputtered to add electrical conductivity to the sensors and wing. d) The UV laser is used to pattern the gold providing electrical isolation between the sensors. The call-out illustration shows a cross-section of 3D printed overhangs that are used for electrical isolation during the deposition of gold.

terms of x_0, y_0, x_f, and y_f as follows,

$$L^2 = x_0^2 + y_0^2 = x_f^2 + y_f^2 \tag{1}$$

We write x_f and y_f as functions of x_0, y_0 and the changes in those components, Δx and Δy as shown in Eq. 2 and 3.

$$x_f = x_0 - \Delta x \tag{2}$$

$$y_f = y_0 - \Delta y \tag{3}$$

L can also be expressed in terms of its initial angle, α, and x_0 as in Eq. 4.

$$L = \frac{x_0}{\cos\alpha} \tag{4}$$

Finally, using the definition of strain and Eq. 1- 4, we obtain the following expression for strain at the top of the sensor in terms of initial geometrical parameters and Δy.

$$\varepsilon_{sensor} = \frac{\Delta x}{x_0} = \frac{x_0 - \sqrt{L^2 - (y_0 - \Delta y)^2}}{x_0} \tag{5}$$

The strain in the substrate can be related to the strain detected by the sensor using Eq. 6, where ρ is the radius of curvature of the bent susbtrate.

$$\rho = -\frac{c}{\varepsilon_{substrate}} = -\frac{c+h}{\varepsilon_{sensor}} \tag{6}$$

Combining Eqs. 5 and 6, we get an expression for the strain measured in the substrate in terms of the sensor's design parameters.

$$\varepsilon_{substrate} = \left[1 - \frac{\sqrt{(x_0/\cos\alpha)^2 - (y_0 - \Delta y)^2}}{x_0}\right]\left(\frac{c+h}{c}\right) \tag{7}$$

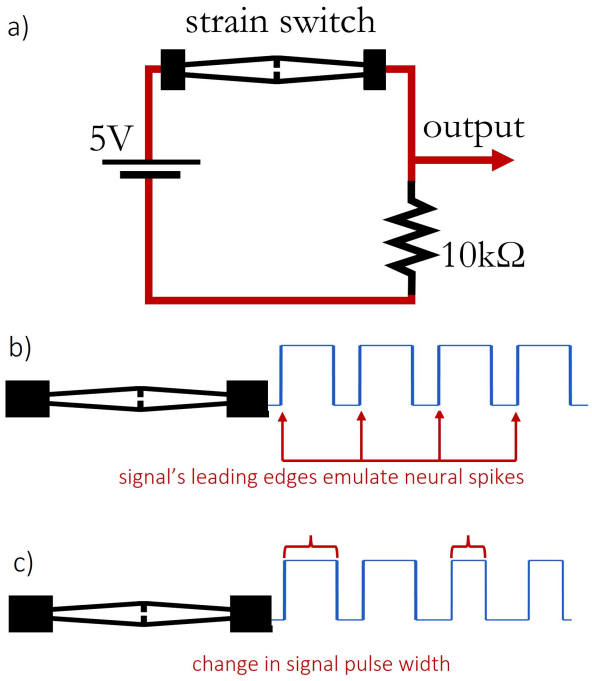

Fig. 5. Circuit diagram and sensor outputs a) The sensor acts as a switch and is incorporated into a voltage divider to generate a digital signal. b) The timing of the leading edge of a single sensor's square wave is similar to neural spikes from biological mechanosensors. c) The pulse width of the 'on'-time of the sensor during each flap cycle can also provide a measure of disturbances on the wing.

C. Fabrication

Fabrication is especially challenging because the sensor must be easily incorporated into a flexible substrate. In addition, the speed of fabrication is important to iterate through sensor designs. The first step in the fabrication starts with a 175 µm thick Indium tin oxide (ITO)-coated PET (polyethylene terephthalate) (Sigma-Aldrich) wing. The PET (sometimes referred to as Mylar) serves as the flexible wing and is similar to previous wings used for flapping flight [14]. The PET is cut and patterned using an LPKF U4 UV laser. In this case, 25 mm x 50 mm rectangular wings are cut to match previous computational work focused on strain sensing in hawkmoth wings [15]. Holes are cut to mount the wing to fixtures for the experimental setup (Fig. 2a). Three fiducials are laser patterned on the top (non-ITO) side of the PET. The fiducials are used as alignment markers during various stages of the fabrication process.

Next, the PET is cleaned using acetone and IPA. A drop of IP-S 2PP resin (Nanoscribe) is placed on a 100 mm diameter 500 µm thick Borofloat 33 glass wafer (University Wafer). The wing is placed ITO side down directly on the IP-S. Capillary forces of the IP-S pull the PET flat for printing. The ITO/IP-S interface provides a contrast of refractive indexes and ensures a strong interface for the Nanoscribe to find [16]. The edges of the wing are secured to the glass wafer using polyimide tape to prevent shifting during printing. Another drop of IP-S is placed on top of the PET to print the sensors.

The sensors are printed using the Dip-In Laser Lithography (DiLL) process with a 25X objective. The ITO/IP-S interface that the Nanoscribe finds is on the bottom of the substrate. Thus, a z-offset must be added to the structures so they print on the top of the PET. The z-offset is dependent on the film thickness and the refractive index at the interface. The z-offset can be easily found by printing alignment crosshairs until they no longer adhere to the PET surface and float away. The z-offset used with this substrate is 182 µm. To ensure proper print quality in between print movements, the settling time of the piezo stage used to adjust to this z-offset was increased to 50 ms. This ensures printing does not start before the piezo is settled. Additionally, the stage velocity was reduced to 50 µm s^{-1} to reduce viscous flow in the resin that can arise from fast stage movements.

Next, a coordinate transformation is completed by using marker alignment to the laser patterned fiducials. The structures are printed, and the PET wing is removed from the glass wafer and developed in PGMEA for 20 min. After development, the wing is rinsed with IPA and dried with a nitrogen spray gun.

To make the wing and 3D structures electrically conductive, gold was sputtered to a thickness of 75 nm using a Perkin Elmer 6J Sputtering System. Electrical isolation is achieved using two different methods. Overhangs are printed directly on the 3D structures that add local electrical isolation (Fig. 2a). Sputtering gold is predominantly a line-of-sight deposition process; during sputtering, the overhangs provide a self-mask that gives local electrical isolation to the sensors (Fig. 4 inset). After sputtering, the sensor is placed in the LPKF laser cutter and aligned to the fiducials. The gold is removed from the PET with a laser power of 0.4 W. This ablation process is used to pattern the larger electrical traces and create global isolation separating the sensors for signal acquisition.

This novel rapid fabricatoin process allows for quick design interation in addition to a robust sensor that has demonstrated a cycle life of greater than 50,000 cycles at 25Hz.

D. Experimental Setup

To generate a signal, the sensors were coupled with a 10 kΩ pull-down resistor to output a square wave during wing flapping (Fig. 5a). A power supply provides 5 V to the circuit. When the switch is open, the output is low, and when a strain threshold has been reached, the switch closes, and the signal changes to a high state.

A quasistatic test of one sensor was carried out to validate the model and ensure the strain threshold was within the maximum strain during flapping. A cantilever deflection test was done to calculate the strain in the PET at the sensor's location. The sensor was printed 2 mm from the base of the wing. A displacement was then applied at a distance $L_2 =$ 6 mm from the base of the wing to bend the wing until a change in the digital signal was observed, indicating that the switch was closed and the strain threshold had been reached. Photos were taken of the wing before and after

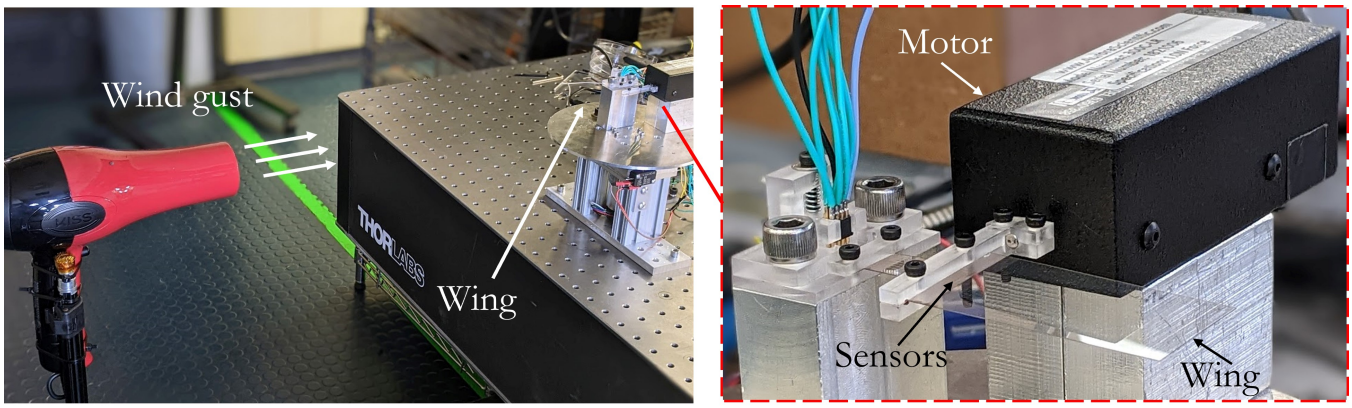

Fig. 6. Wind disturbance experimental setup. A hair dryer was used to generate a wind gust of 3 m/s to provide a disturbance to the flapping wing. The call-out shows the flapping wing setup. The wing was mounted to an Aurora motor, and a 25Hz + 50Hz flapping signal activated the motor.

the displacement to photogrammetrically calculate the total applied displacement, δ. The strain was calculated at the sensor displacement using the following equation:

$$\varepsilon = \frac{3\delta L_1 t}{2L_2^3} \tag{8}$$

Where $L_1 = 4\,\text{mm}$ is the distance from the point of displacement to the sensor and t is the thickness of the substrate (175 µm). It should be noted that this linear elastic model is not accurate for large deflections.

Next, three sensors with different designed thresholds were used to test the general response of the sensor on a flapping wing and demonstrate how the signal timing can be affected through sensor design. The three sensors were centered along the chord and placed 2 mm from the base of the wing. The sensors were connected to the digital pins on an Arduino UNO microcontroller, and the wing was flapped at a frequency of (5 Hz).

The third experiment was designed to demonstrate the effect of wind disturbances on the sensors' activation timing. A PET wing was designed with a sensor centered along the chord of the wing. This wing was then attached to the shaft of an Aurora Scientific Model 300C-LR Dual-Mode Lever Arm system (Fig. 6). The flapping motion of a hawkmoth's wing can be modeled as the sum of two sine waves [15]. A signal was generated with a primary frequency of 25 Hz with a 15° flapping amplitude (A_1) and a secondary frequency of 50 Hz with 20% of the primary amplitude, A_2.

$$signal = A_1 * \sin(2\pi * 25t) + A_2 * \sin(2\pi * 50t) \tag{9}$$

The signal was generated in MATLAB and output to the Lever Arm's length driver via a National Instruments X-Series DAQ (Fig. 6b). To sample the sensor's signal, a spring-loaded connector was used to make contact with the conductive traces. The signal was read with the digital input on the NI DAQ at a sampling rate of 1 MHz.

A hair dryer was used to create a $3\,\text{m}\,\text{s}^{-1}$ wind disturbance (Fig. 6). The hair dryer was attached to a tripod and placed level with the wing. A hot-wire anemometer was used to measure the average velocity of the wind gust. A barrier was placed in front of the hair dryer and removed during the flapping wing cycle to produce a wind gust.

Sensor data was collected from one sensor during flapping only as well as flapping plus a wind disturbance. Two methods were used to evaluate timing differences when a disturbance was added. In the first, the timing of the rising edge was noted as may be captured using a microcontroller interrupt function (Fig. 5b). This approach is also similar to the spiking in the campaniform sensilla. The second approach simply measured the pulse width of the 'on'-time of the sensor to look for changes that might indicate a disturbance (Fig. 5c).

III. Results and Discussion

A. Quasistatic test and Model Comparison

After gold is deposited during the fabrication process, residual stresses remain in the substrate and the sensors. This residual stress adds an unwanted pre-strain to the wing and the sensors. As a result, the dimensions of the fabricated sensor can be significantly different from the design. Instead of using the designed parameters of the sensor in this test to confirm the accuracy of the analytical model, the sensor's fabricated dimensions were obtained using a confocal microscope (Zeiss LSM400). These dimensions were used in the analytical model and gave a theoretical strain threshold of 3.25 millistrain. The results from the quasistatic test indicated an activation at 3.4 millistrain. These numbers show agreement between the model and the experimental results and provide a general guideline for sensor design. It's important to note that there is no mapping between the sensor and strain threshold, but instead the focus is when changes are happening through the modulation of pulses generated by the sensor.

B. Three Sensor Threshold

The timing of the output of the sensor can be varied using different sensor designs to target different strain thresholds. Three sensors were designed with theoretical strain

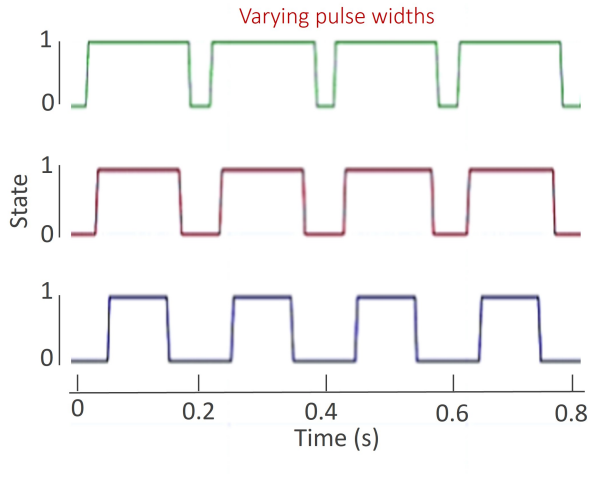

Fig. 7. Digital signals from three sensors designed with different strain sensing thresholds. The changing pulse widths indicate that the threshold strain is sensed at different points within the flap cycle.

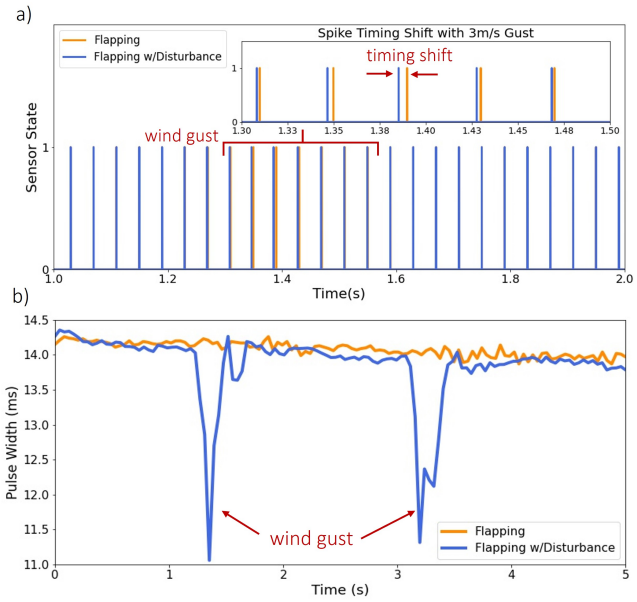

Fig. 8. Wind disturbance data. a) The spike timing of one sensor is shown with a 3 m/s wind gust. The wind gusts cause slight changes in the activation timing of the sensor. b) The gust is detected by analyzing the pulse width timing from the strain threshold sensor. The wind gust causes a noticeable change in this pulse width timing.

thresholds of 3000, 3500, and 4000 microstrain, although as indicated in the quasistatic results, the fabricated strain thresholds differed significantly from the designs. The sensors were tested on a wing with a flapping frequency of 5 Hz. Fig. 7 shows the effect of changing the target threshold to achieve pulse width modulation of the sensor output. Even though the strain thresholds in the fabricated sensors differed from the designs, the trends remained.

C. Detecting disturbances with rising edge

A single sensor was tested with flapping only and flapping with a 3 m/s wind disturbance. The timing of the rising edge of the square wave was measured and plotted to emulate the action potentials of the hawkmoth (Fig. 8)a. When the wind gust is introduced, the flapping cycle of the wing is changed, which affects the timing of the sensor responses and can be seen as a shift from the expected timing of the sensor activation.

D. Detecting disturbances with pulse width

Next, the pulse width of the sensor's digital output was plotted. In this case, the pulse width represented approximately one third of a total wingbeat period at approximately 14 ms when no disturbance was applied. The applied wind disturbance is shown as a clear deviation from the nominal pulse width in Fig. 8b.

IV. Conclusion and Future Outlooks

This work presented a novel digital strain sensor to evaluate the strain threshold timing of a flapping wing. The sensor was inspired by campaniform sensilla found on the wings of insects that generate neural spikes in response to strain in the wing. The bio-inspired sensor acts as a switch and outputs a low latency digital signal when used with a pull-down resistor. Furthermore, the microscale sensors can be easily incorporated on relatively large (2.5 cm x 5 cm) wings using microscale 3D printing via two-photon polymerization.

An analytical model was used to target a particular strain threshold based on the design parameters. While film stress introduced during fabrication changed the dimensions of the fabricated sensors, trends in the model were validated through testing. Future work can focus on compensating for this film stress in either the model or fabrication process. The sensorized wing was flapped at 25 Hz and subjected to a $3\,\mathrm{m\,s^{-1}}$ wind disturbance easily detected using only one sensor.

Using this novel approach of digital sensing to evaluate timing may provide low latency detection of flight disturbances providing event based that is usefule in rejecting these disturbances through feedforward control. Biologists hypothesize that flying insects may use the campaniform sensilla to detect inertial forces due to movements during flight [17]. Future work will include strain threshold characterization and testing of the sensors bandwith. In addition, we will evaluate the timing difference between sensors on a flapping wing when subjected to the principal flight rotations of yaw, pitch, and roll to determine if digital strain sensors can be used to distinguish between these inertial movments.

Acknowledgment

The authors would like to thank the staff of Claire & John Bertucci Nanotechnology Laboratory and Soft Lithography lab at Carnegie Mellon University for their assistance in microfabrication and 3D printing. The authors would also like to thank Bram Miller for his help with fabrication and F. Zeynep Temel for allowing the use of her lab. A special thanks to Bing Brunton and Tom Daniel for their insightful discussions and feedback that helped shape this project.

REFERENCES

[1] J. Zhang, F. Fei, Z. Tu, and X. Deng, "Design optimization and system integration of robotic hummingbird," in *2017 IEEE International Conference on Robotics and Automation (ICRA)*. IEEE, 2017, pp. 5422–5428.

[2] M. Karásek, F. T. Muijres, C. De Wagter, B. D. Remes, and G. C. De Croon, "A tailless aerial robotic flapper reveals that flies use torque coupling in rapid banked turns," *Science*, vol. 361, no. 6407, pp. 1089–1094, 2018.

[3] R. Wood, R. Nagpal, and G.-Y. Wei, "Flight of the robobees," *Scientific American*, vol. 308, no. 3, pp. 60–65, 2013.

[4] S. P. Sane, A. Dieudonné, M. A. Willis, and T. L. Daniel, "Antennal mechanosensors mediate flight control in moths," *science*, vol. 315, no. 5813, pp. 863–866, 2007.

[5] A. J. Hinterwirth and T. L. Daniel, "Antennae in the hawkmoth manduca sexta (lepidoptera, sphingidae) mediate abdominal flexion in response to mechanical stimuli," *Journal of Comparative Physiology A*, vol. 196, no. 12, pp. 947–956, 2010.

[6] A. Dahake, A. L. Stöckl, J. J. Foster, S. P. Sane, and A. Kelber, "The roles of vision and antennal mechanoreception in hawkmoth flight control," *Elife*, vol. 7, p. e37606, 2018.

[7] Dombrowski UJ, "Untersuchungen zur funktionellen Organisation des Flugsystems von Manduca sexta (L.)," Ph.D. dissertation, Universitaet zu Koeln, 1991.

[8] T. L. Mohren, T. L. Daniel, S. L. Brunton, and B. W. Brunton, "Neural-inspired sensors enable sparse, efficient classification of spatiotemporal data," *Proceedings of the National Academy of Sciences*, vol. 115, no. 42, pp. 10 564–10 569, Oct. 2018. [Online]. Available: http://www.pnas.org/lookup/doi/10.1073/pnas.1808909115

[9] B. H. Dickerson, Z. N. Aldworth, and T. L. Daniel, "Control of moth flight posture is mediated by wing mechanosensory feedback," *Journal of Experimental Biology*, vol. 217, no. 13, pp. 2301–2308, 2014.

[10] H.-S. Shin, L. M. Castano, J. S. Humbert, and S. Bergbreiter, "Sensing skin for detecting wing deformation with embedded soft strain sensors," in *2016 IEEE SENSORS*. IEEE, 2016, pp. 1–3.

[11] L. M. Castano, G. M. Gremillion, A. E. Winkelmann, and J. S. Humbert, "Disturbance rejection for an unmanned rotary aircraft system using strain sensing," *Journal of Guidance, Control, and Dynamics*, vol. 42, no. 12, pp. 2638–2649, 2019.

[12] E. Farrell Helbling and R. J. Wood, "A review of propulsion, power, and control architectures for insect-scale flapping-wing vehicles," *Applied Mechanics Reviews*, vol. 70, no. 1, 2018.

[13] J. Guo, M. Suster, D. J. Young, and W. H. Ko, "High-gain mechanically amplified capacitive strain sensor," in *SENSORS, 2005 IEEE*. IEEE, 2005, pp. 4–pp.

[14] P. J. Lane, I. Fernandez, G. Throneberry, and A. Abdelkefi, "Sizing process and manufacturing of an optimal flapping wing micro air vehicle," in *AIAA Aviation 2019 Forum*, 2019, p. 3239.

[15] A. I. Weber, T. L. Daniel, and B. W. Brunton, "Wing structure and neural encoding jointly determine sensing strategies in insect flight," *PLoS Computational Biology*, vol. 17, no. 8, p. e1009195, 2021.

[16] Y. Lin, R. Zhou, and J. Xu, "Superhydrophobic surfaces based on fractal and hierarchical microstructures using two-photon polymerization: toward flexible superhydrophobic films," *Advanced Materials Interfaces*, vol. 5, no. 21, p. 1801126, 2018.

[17] A. L. Eberle, B. H. Dickerson, P. G. Reinhall, and T. L. Daniel, "A new twist on gyroscopic sensing: body rotations lead to torsion in flapping, flexing insect wings," *Journal of The Royal Society Interface*, vol. 12, no. 104, pp. 20 141 088–20 141 088, Jan. 2015.